ELSEVIER

Journal of Alloys and Compounds 258 (1997) 61–73

Journal of ALLOYS AND COMPOUNDS

# Actuators, transducers and motors based on giant magnetostrictive materials

F. Claeyssen[a,*], N. Lhermet[a], R. Le Letty[a], P. Bouchilloux[b]

[a]*Cedrat Recherche, Zirst, F38246 Meylan Cedex, France*
[b]*Magsoft Corporation, 1223 People's Avenue, New York NY 12180, USA*

Received 6 November 1996; revised 23 January 1997

**Abstract**

Rare earth–iron magnetostrictive alloys, especially Terfenol-D, feature "giant" magnetostrains: static strains of 1000–2000 ppm and dynamic strains of 3500 ppm are reported. These strains permit building various actuating devices (actuators, transducers, motors) both at macro and micro scale. The object of the paper is to recall adapted design methods, especially finite element methods such as ATILA, and to review these different kinds of devices studied at Cedrat Recherche, providing both up-dated experimental and numerical results. The presented devices will include several large displacement longitudinal and shear actuators biased using permanent magnets and used either as characterisation devices or as electromechanical actuators (for active damping, for sonar transducers...), a 1 kHz 4 kW Tonpilz-type sonar transducer called the Tripode, a 2 N m torque rotating Multi-Mode Motor, a torsion based drift free micro actuator and a wireless linear micromotor. © 1997 Elsevier Science S.A.

*Keywords:* Magnetostriction; Actuator; Transducer; Motor; Experiment; Modelling

## 1. Introduction

Magnetostriction occurs in the most ferromagnetic materials and leads to many effects [1,2]. The most useful one is referred to as the Joule effect. It is responsible for the expansion (positive magnetostriction) or the contraction (negative) of a rod subjected to a longitudinal static magnetic field. In a given material, this magnetostrain is quadratic and occurs always in the same direction whatever the field direction.

Rare earth–iron "giant" magnetostrictive materials (GMM) discovered by A.E. Clark [3], feature magnetostrains which are two orders of magnitude larger than nickel. Among them, $Tb_{0.3}Dy_{0.7}Fe_{1.9}$, often called Terfenol-D, presents, at room temperature, the best compromise between a large magnetostrain and a low magnetic field. Positive magnetostrains of 1000–2000 ppm obtained with fields of 50–200 kA $m^{-1}$ are reported for bulk materials [3,4]. New composite materials of Feredyn offer an interesting possibility for high frequency ultrasonic applications [5]. More recently, high magnetostrains (in the range of 500–1000 ppm) have also been obtained in rare earth–iron thin films [6]. However, these expansion strains are rarely used directly because most applications require a linear behaviour. The linearity is obtained by applying a magnetic bias and a mechanical prestress in the active material. Moreover, in the case of applications based on a mechanical resonance, it is a condition to produce "giant" dynamic strains, the peak-to-peak amplitude of which is higher than static magnetostrain [7].

The static magnetostrain of this material permits building linear actuators offering large displacements (20–200 μm) and large forces (500–5000 N) at low voltage. These linear actuators are studied to be used directly, for instance, for micro positioning tools or for damping structures. They can also be used as components of a more complex actuator, such as inchworm motors. Thus, these motors present holding forces/torques which are often much higher than piezoelectric inchworm motors. They also present a good positioning accuracy. Their main disadvantage is a low efficiency, due to the static operating conditions.

The giant dynamic strains (up to 3500 ppm) can be produced in Terfenol-D linear actuators using the device mechanical resonance, even against high load working. In such conditions, very large powers and rather good efficiency can be achieved. Using these properties, some

*Corresponding author.


*PII* S0925-8388(97)00070-4

magnetostrictive underwater transducers already out-perform PZT transducers in the low-frequency domain and receive a great deal of attention. Some research works are being pursued in order to also use mechanical resonance in magnetostrictive motors, aiming for a higher mechanical power and a better efficiency than in inchworm motors.

Although there is no large scale application at the moment, some devices are already used for specific applications in domains like pumps, micro-positioners, transducers, and research in applications is growing. It is likely to see magnetostriction also finding applications in the micro-actuators domain in the future.

## 2. The theory of magnetostriction in GMM devices

### 2.1. The GMM constitutive laws

In the most general way, the behaviour of magnetostrictive materials is non-linear [1,2] and has to be described with non-linear relations:

$$\begin{cases} S = \mathrm{f}(T,H) \\ B = \mathrm{g}(T,H) \end{cases} \tag{1}$$

relating $S$ and $T$ the tensors of strain and stress to $B$ and $H$ the vectors of the induction and magnetic field. The functions f and g may be obtained by measuring the magnetostriction and the magnetization versus the applied field and the external stress [8]. Then the functions f and g can be described numerically by an interpolation method [9,10]. This technique is used in the SANDYS software based on a finite difference method [11] for modelling 2D structures. Another method could consist in developing f and g as a Fourier series taking some first order terms. Such an approach is being applied in the ATILA software based on a finite element method [12], for modelling the non-linear behaviour of 3D structures including electrostrictive materials [13].

However, though magnetostrictive materials are non-linear, the behaviour of most of the magnetostrictive devices may be rather well described using a linear theory, because the active materials are biased. Experimental results obtained on a high power transducer (Section 3.2) show that linearity can be rather good even with large excitation fields and large dynamic strains.

The bias conditions are defined by the magnetic bias $H_o$ and the mechanical pre-stress $T_o$, applied along the magnetostrictive rod axis, referred to as the third axis.

Then, considering only the variations around this initial bias state, the material behaves in a quasi-linear manner and follows piezomagnetic laws [14]:

$$\left\{ \begin{array}{l} S_i = s_{ij}^H T_j + d_{ni} H_n \\ B_m = d_{mj} T_j + \mu_{mn}^T H_n \end{array} \right. \left| \begin{array}{l} i,j = 1,\ldots,6 \\ m,n = 1,\ldots,3 \end{array} \right. \tag{2}$$

where $s^H$, $d$ and $\mu^T$ are the tensors of constant-$H$ compliance, piezomagnetic constants and constant-$T$ permeabilities, respectively. They are called the magneto-elastic coefficients.

$S$ and $T$ are the tensors of varying strain and stress, $B$ and $H$ are the vectors of varying induction and magnetic field. In the actuators, $H$ is called the excitation field.

The real situation in the material can be reconstructed by adding the bias static situation to the variations. For instance, the real field in the material is the vectored sum of static magnetic bias $H_o$ and the varying magnetic field $H$.

Three other equivalent systems can be written according to the chosen state variables. For instance, instead of $T$ and $H$, the following system uses $S$ and $H$ as the independent variables:

$$\left\{ \begin{array}{l} T_i = c_{ij}^H S_j - e_{ni} H_n \\ B_m = e_{mj} S_j + \mu_{mn}^S H_n \end{array} \right. \left| \begin{array}{l} i,j = 1,\ldots,6 \\ m,n = 1,\ldots,3 \end{array} \right. \tag{2b}$$

The grain oriented Terfenol-D, which is isotropic in the plane perpendicular to the average grain axis, can be classified into the 6 mm crystal class, which leads to a particular distribution of zero magneto-elastic coefficients [14]. Note that the values of the non-zero coefficients depend strongly on the bias and the prestress [14,8]. Complete sets of values for the tensors $s^H$, $d$ and $\mu^T$ and for the tensors $c^H$, $e$ and $\mu^S$ of Terfenol-D have already been established [14–16]. Longitudinal coefficients ("33") and shear coefficients ("15") may be determined using length expansion and shear resonators such as MB [15] and DCC [17] of Fig. 1. Other coefficients may be found using some special assumptions [14].

Terfenol-D is often used in long rod, subjected to an excitation field parallel to the rod axis. In this case, the simple theory of the longitudinal mode can be applied. Such theory can be used to get a preliminary design, before the use of numerical models.

In such a situation, it is supposed that the transverse excitation fields are negligeable ($H_1 = H_2 = 0$). In theory a pure longitudinal mode ("33" mode) is obtained starting from the assumption that radial stresses are equal to zero ($T_1 = T_2 = 0$) and there is no shear effect ($T_4 = T_5 = T_6 = 0$), leading to the following equations:

$$\begin{cases} S_1 = S_2 = s_{13}^H T_3 + d_{31} H_3 \\ S_3 = s_{33}^H T_3 + d_{33} H_3 \\ B_3 = d_{33} T_3 + \mu_{33}^T H_3 \end{cases} \tag{3}$$

The "33"-mode coupling coefficient associated with this mode is given by the following expression:

$$k_{33}^2 = \frac{d_{33}^2}{s_{33}^H \mu_{33}^T} \tag{4}$$

This coefficient represents the capability of the material to convert electric energy into elastic energy. According to recent experimental results (Table 1) obtained using a dual

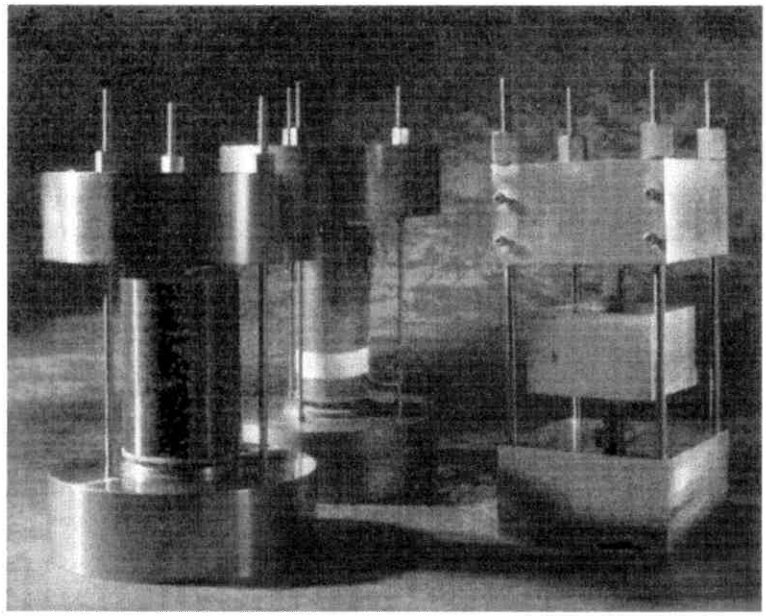

Fig. 1. MB, MAS and DCC actuators.

mass resonator [15] and in agreement with other methods [8], its value is high in Terfenol-D even with high prestress and bias. As will be shown further on, the combination of a high coupling, a high prestress and a high bias is required to obtain giant dynamic strains and very high output powers [7].

### 2.2. A simple theory

It is interesting to analyse the behaviour of linear actuators because most applications are based on such actuators. To simplify the presentation, one must consider an actuator with one end working either in the air (no load) or against a purely resistive load ($R_{load}$). The other end of the actuator is clamped. The vibration against this load produces an output power (either mechanical or acoustic). Its behaviour is representative of any magnetostrictive device to have to produce an output power. Most of them can be analysed as systems including a compliance $k^H$ (at constant field), an effective mass $M$ and a mechanical resistance $R_m$ due to internal mechanical losses. The magnetostrictive part is activated by a longitudinal field $H_3$ produced by a coil driven by an excitation current $I$. In such a system, all the strain is converted to displacement of the free mass.

Under quasi-static conditions, according to Eq. (3) and neglecting prestress spring stiffnesses for a first approximation (which gives $T_3=0$), the strain $S_3$ of Terfenol-D in an unloaded actuator is:

$$S_3 = d_{33}H_3 \tag{5}$$

A maximum excitation field $H_3$ equal to the bias $H_o$ can be applied. Higher values lead to frequency doubling effect. In this situation, the actuator is field-limited. The heating of the coil is another limitation often encountered in static conditions. High excitation field needs a high current density in the coil wires, typically in the range of 10 A mm$^{-2}$. As it is a rather high value, significant heating may occur and it is therefore necessary either to use the actuator during short pulses or to cool the coil.

When the unloaded actuator is excited with a constant field amplitude versus frequency, a sharp peak of vibration is obtained. A quite typical example of strain curves (Fig. 2) without load and with a load $L=1^{E4}$ rayls is given by a linear Terfenol-D actuator with a driver such as MAP described in Section 3.2. The natural longitudinal vibration mode occurs. Due to the coupling, this mode is magnetically excited. So compared to static strains, the strains at resonance are magnified by a factor called the device mechanical quality factor $Q_m$ (the load $L=1^{E4}$ rayls of the example being equivalent to $Q_m=2$):

$$S_3 = Q_m d_{33}H_3 \tag{6}$$

Table 1
Magnetoelastic longitudinal coefficients of Terfenol-D at about 90 kA m$^{-1}$ bias versus prestress $T_o$

| $T_o$ (MPa) | 30 | 35 | 40 | 50 |
|---|---|---|---|---|
| $Y^H$ (GPa) | 29 | 21 | 23 | 40 |
| $s_{33}^H$ (GPa$^{-1}$) | 0.034 | 0.048 | 0.043 | 0.025 |
| $Q^H$ | 4.6 | 3.5 | 4.3 | 8.3 |
| $\mu_{33}^T/\mu_o$ | 3.7 | 4.2 | 3.8 | 3.0 |
| $Q^T$ | 2.0 | 1.9 | 2.2 | 2.8 |
| $d_{33}$ (nm A$^{-1}$) | 8.0 | 11.0 | 9.7 | 5.0 |
| $k_{33}$ (%) | 63.1 | 69.3 | 67.4 | 52.0 |

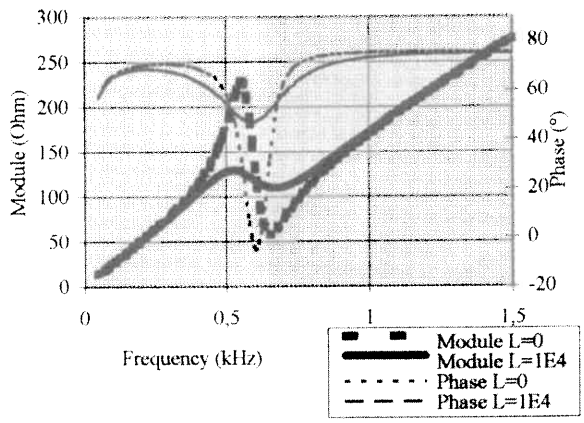


Fig. 2. Impedance versus frequency without load and with a load equivalent to $Q_m = 2$.

This mechanical quality factor defines the damping of the resonance. When the vibrating end is unloaded, the damping is only due to internal mechanical losses and $Q_m$ is equal to the material mechanical quality factor $Q^H$. When a load is applied, the resistive part of the load provides an additional damping which reduces the device mechanical quality factor. Typical values for $Q^H$ in Terfenol-D are in the range from 3 to 20. Consequently, for a very first approximation, the maximum strain $S_3$ at resonance under such condition is determined from Eq. (3) and Eq. (6), by the stress $T_3$, since $d_{33}H_3$ is necessarily small compared with $s^H_{33}T_3$:

$$S_3 = s^H_{33}T_3 \tag{7}$$

Without load (or also with a small load), the actuator is limited at resonance by the stress: the dynamic stress level $T_3$ reaches the prestress value $T_o$. So using a high prestress, the maximum dynamic peak-to-peak amplitude of strain may be much higher than the maximum static strain (1600 ppm for this material) [7]. For instance with $T_o = 40$ MPa, the peak-to-peak strain is about $S_{pp} = 2.S_3 =$ 3500 ppm according to Eq. (7) and Table 1. This high strain is also permitted by the good coupling factor of Terfenol-D at such high prestress. Due to this good coupling, this strain is obtained under low load with a low field peak amplitude $H_3 = 40$ kA m$^{-1}$ according to Eq. (6) and Table 1. Intensive research on giant strains is being conducted and has permitted the experimental exploration of peak-to-peak strains of 3500 ppm and more (Section 3.1).

Due to the strong coupling, the mechanical resonance obtained at constant current is associated to the electrical antiresonance $f_a$: the maximum impedance (Fig. 2). Using a constant voltage, the mechanical resonance would occur at the electrical resonance $f_r$: the minimum impedance. These resonances determine the effective coupling factor $k_{eff}$ of the device:

$$k_{eff} = \sqrt{1 - (f_a/f_r)^2} \tag{8}$$

This factor represents the capability of the device to convert electric energy to elastic energy. As shown below, the output power of a device depends strongly on this factor. In the best theoretical case, it is equal to the material coupling factor. In the best actuators, the measured $k_{eff}$ may reach 55–60%.

The high-power handling capability of Terfenol-D can be observed by applying a high load. A high load condition is achieved when the mechanical quality factor $Q_m$ of the vibration mode of the system is low (load higher than the optimal load). In this case, the actuator is field-limited, even at resonance. Then the maximum excitation field which can be applied is equal to the bias. It is important to notice that even against such high loads and unlike the PZT actuators in a same condition, the maximum strain of Terfenol-D actuators remains very high (Fig. 3).

A special case is obtained with an optimal load. Both stress and field limits are reached. This permits production of the absolute maximum power. The optimal load of an actuator can be determined theoretically. Typically (Table 2, Section 3.2), it leads to a mechanical quality factor in the range 2 to 3, which also shows the ability of Terfenol-D to work against high load.

The output power can be compared to the electric power through the efficiency (Fig. 4). The curve of efficiency versus frequency shows that the best way to produce a significant output power with an actuator or a transducer is to work at resonance. A good efficiency ($\geq$50%) may be obtained with a high load ($Q_m \leq 2$).

The expression of the output power at resonance [14] permits examination of the role of some parameters:

$$P_{output} = \omega e_m k^2_{eff} Q_m \left(\tfrac{1}{2} L_{LF} I^2\right) \tag{9}$$

where $(L_{LF}I^2/2)$ is the electric energy stored in the low frequency inductance of the device, $e_m = 1/(1 + R_m/R_{load})$ is a mechanical efficiency and $\omega$ is the resonance pulsation. In general, the pulsation and the load are often

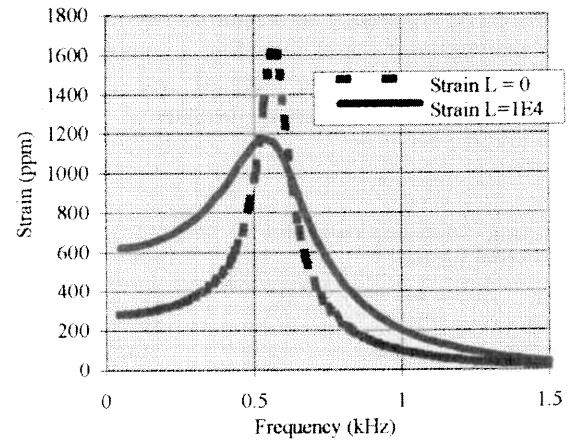


Fig. 3. Strain versus frequency at constant currents, without load and with a load equivalent to $Q_m = 2$.

Table 2
Experimental properties of the MB, MAP, MAS drivers

| | | | M.B. | M.A.P. | M.A.S. |
|---|---|---|---|---|---|
| Bias | $H_o$ | (kA m$^{-1}$) | 100 | 90 | 90 |
| Prestress | $T_o$ | (MPa) | 30 | 40 | 35 |
| Coupling coefficient | $k_{eff}$ | (%) | 52 | 55 | 35 |
| Max. magnetic energy density | $\epsilon'_m$ | (kJ m$^{-3}$) | 6.3 | 3.0 | 4.0 |
| Max. elastic energy density | $\epsilon'_e$ | (kJ m$^{-3}$) | 15.3 | 30 | 48.5 |
| Max. dynamic strains | $S_{pp}$ | (ppm) | 2020 | 3000 | 3500 |
| Optimal mechanical quality factor | $(Q_m)_{opt}$ | | ≈1.5 | ≈ 2.5 | ≈3.5 |
| Max. dissipated energy density | $(\epsilon'')_{opt}$ | (kJ m$^{-3}$) | ≈10 | ≈10 | ≈12 |

prescribed by the application. When it is possible to select the load, a high load is preferred to obtain a high efficiency. The stored electric energy can be increased using higher prestress, bias and current. However, bias values much greater than 100 kA m$^{-1}$ are difficult to produce with permanent magnets. The effective coupling factor can be optimised working on the design.

The maximum force that can be produced by the actuator is the clamped force. This force $F$ is given by $G$, the force factor also called the electromechanical conversion factor:

$$F = GI \tag{10}$$

with:

$$G = k_{eff}\sqrt{L_{LF}k^H} \tag{11}$$

This is also the blocked force of the main mode of the actuator at resonance. So, it is an important parameter for several applications. For example, in both quasi-static and resonant motors, it influences strongly the maximum force/torque of the motors.

This simplified theory provides an understanding of some important features of linear magnetostrictive drivers of actuators, transducers, etc.. It shows for instance that a driver may be limited either by the stress or by the field, and that the strain at resonance may be much larger than that of static and may require much less field. However, because of the assumptions on the field shape, the strain uniformity and so on, it cannot predict accurately the behaviour of the device, especially its exact limits. So, without a good knowledge of these limits, it is difficult to use the full potential device. That is why a more accurate model is required and has been developed.

### 2.3. A variational principle of GMM devices

An accurate description of the behaviour of magnetostrictive devices implies to take into account mechanical, magnetic and electrical states in a consistent way and without any assumption on the device geometry and the solution.

This can be performed at first by applying the Euler equations in any point of the device:

- The Newton's law (for the mechanical domain, including magnetostrictive parts)
- The magnetic flux conservation (for the magnetic domain, including magnetostrictive parts and vacuum surrounding the device)
- The Ampere's law (for the electric domain: the currents into the excitation coils).

These equations are local and do not depend on the

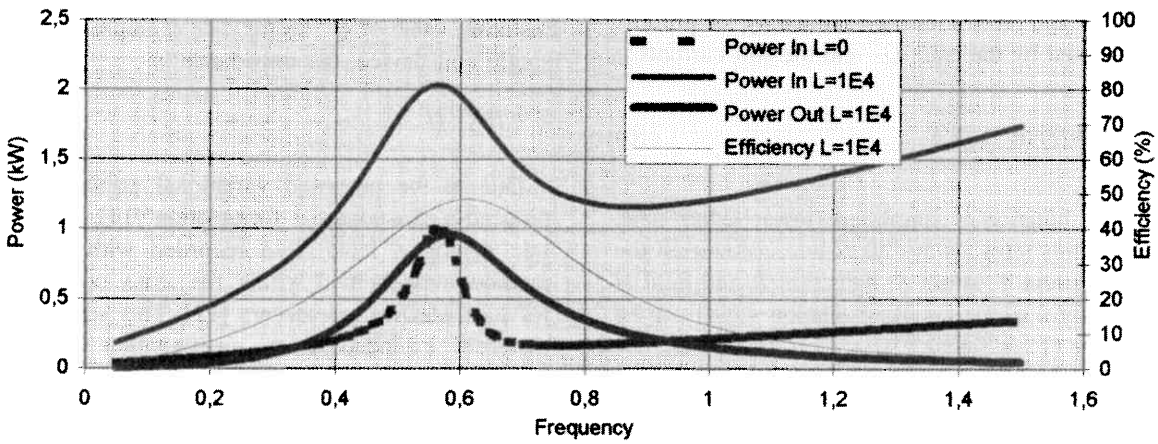


Fig. 4. Powers and efficiency versus frequency without load and with a load $L$ equivalent to $Q_m = 2$.

materials constitutive Eqs. (1) and (2), which have to be taken into account in addition.

A second way, called variational principle, relies on the stationary nature of a quadratic functional **L** (a kind of energy minimisation) with respect to the state variables. A satisfying variational principle has to be mathematically equivalent to the previous Euler equations and has to take into account the boundarie conditions. The chosen state variables are in this problem the displacement field $u$, the reduced scalar potential $\phi$ of the magnetic field and the set of currents $I$ in the coils.

For this problem, it can be shown that a satisfying variational principle is simply an extension of the Hamilton principle [14,15]. The stationary quantity **L** is equal to a generalised Lagrangian $L$ added to a sum of virtual works $W$. It is calculated on the volume $V$ of the domain, defined by the device and the vacuum around the device, where the field is not zero.

$$\mathbf{L} = L + W \tag{12}$$

The stationary condition is obtained for small variations $\delta$ around the solution which can be written as following:

$$\delta \mathbf{L} = 0 \tag{13}$$

The generalized Lagrangian $L$ is defined by the difference between the kinetic energy $E_c$ and the magnetic enthalpy $H$.

$$L = E_c - H \tag{14}$$

The kinetic energy term can be written differently according to the type of analysis (static, harmonic, transient). For example in static analysis it is equal to 0 and in harmonic analysis at pulsation $\omega$ it is an integral depending on the displacement field $u$ and the local density $\rho$:

$$E_c = \int_V \frac{1}{2}\rho\omega^2 u^2 \mathrm{d}V \tag{15}$$

The enthalpy term includes internal mechanical energy, magnetic energy and electric energy defined by the product of fluxes generated by the coils $Q^V$ and the coil currents $I$.

$$H = \int_V (\tfrac{1}{2}TS - \tfrac{1}{2}BH)\,\mathrm{d}V + Q^V I \tag{16}$$

Although the notation is simplified (lower letters have been dropped), this term always takes into account all the components of stress $T$, strain $S$, induction $B$ and field $H$ that are bound by a strong coupling relation which can be either non-linear (1) or linear (2).

The virtual works $W$ is the sum of the mechanical works done by the prescribed normal forces $T_N$ on the surface $S_T$ and the works done by the prescribed induction $B_N$ on the surface $S_B$.

$$W = \int_{S_T} T_N u \mathrm{d}S + \int_{S_B} B_N \phi \mathrm{d}S. \tag{17}$$

Note that all these equations can be used not only for the magnetostrictive materials but also for the whole magnetostrictive device including the air around it. Then the coupling terms between elastic tensors $(S,T)$ and magnetic vectors $(H,B)$ are simply zero.

This thermodynamic interpretation of the proposed variational principle ensures for the method the existence and the uniqueness of the solution.

### 2.4. A finite element method for magnetostrictive devices

The main advantage of a variational principle is its global approach (at the opposite of the Euler's equations which are local) which permits the problem to be treated by a finite element method (FEM). Thus the resolution of the 3D magnetostrictive problem is equivalent, when discretized using the FEM, to the numerical resolution of a linear system, the unknown of which are the state variables $u$, $\phi$ at the nodes of the mesh and the coils flux $Q^V$. For example, in harmonic analysis (and in static with $\omega = 0$) the system is as follows:

$$\begin{bmatrix} [K_{uu}] - \omega^2[M] & [K_{u\phi}] & [K_{uI}] \\ [K_{u\phi}]^T & [K_{\phi\phi}] & [K_{\phi I}] \\ [K_{uI}]^T & [K_{\phi I}] & [K_{II}] \end{bmatrix} \begin{bmatrix} u \\ \phi \\ I \end{bmatrix} = \begin{bmatrix} F \\ Q \\ -Q^V \end{bmatrix} \tag{18}$$

The vectors of force $F$ and fluxes $Q$ are equal to 0, but, respectively, on prescribed displacements $u$ and potentials $\phi$ which occurs on Dirichlet-type boundaries, then they are unknown. In prescribed current analysis the set of currents $I$ is known. When this system is solved, one can deduct for example the strains from the displacements, the magnetic field from the potentials and the currents (reduced-scalar potential method), then the stress field and the induction field from Eq. (1). The inductances are given by the resulting value of $Q^V$ vector. For example, in the case of a single coil device, the impedance is:

$$Z = j\omega Q^V / I \tag{19}$$

Due to the proposed variational principle and to the reduced-scalar-potential formulation [14], strong algorithmic analogies have been recorded with respect to the method implemented within the ATILA computation code for piezoelectric transducers [12]. This software has been therefore extended to the computation of 2D and 3D magnetostrictive transducers [18] under advantageous conditions. Different types of resolutions have been developed: Constant-current, quasi-static, harmonic or modal analysis (Antiresonances and resonances). It has been used

at first for the analysis of magnetostrictive transducers and actuators [16,19]. Then, it has been demonstrated that it permits the analysis of piezoelectric and magnetostrictive friction motors [20–22]. At last, a 3D transient solver has also been implemented.

## 3. The principles and the properties of various applications

### *3.1. Linear actuators and drivers*

Many linear actuators have been built [23–30]. For example, Etrema has a wide range of products of different sizes, which are adapted to a quasi-static use. The 50/6MP for instance [23] is based on a 50 mm-long 6 mm-in diameter Terfenol-D rod. It is biased with a field $H_0$ of about 40 kA $m^{-1}$. Low prestress and bias have the advantage of yielding to the highest $d_{33}$ values. Consequently, due to Eq. (5), a high static strain $S_3$ of the unloaded actuator is obtained with a small field $H_3$. The maximum static strain of 500 ppm leading to a displacement of 25 μm can be achieved with a field of about 35 kA $m^{-1}$. It gives a strain of 14 ppm per kA $m^{-1}$. It is better than that of the MAP actuator of Cedrat Recherche which offers only 7 ppm per kA $m^{-1}$. On the other hand, the prestress $T_0$ of 50/6MP is lower than 20 MPa, so much smaller than that of MAP. So the maximum dynamic strain of 50/6MP is limited to about 1000 ppm and is also much smaller than that of MAP that reaches more than 3000 ppm. This example shows that each actuator should be designed for its specific application.

The design problem of magnetostrictive linear driver has been addressed at Cedrat through several actuators (Fig. 1) [16,31,22]. These actuators are identical except in their bias system. They are all based on one driver and two symmetrical head-masses. Their driver contains a total length of Terfenol-D of 100 mm. The rod diameter is 20 mm. The first actuator, called MB, is biased with a DC current in a coil giving a bias field from 0 to 160 kA $m^{-1}$. The second one, MAP, is biased with permanent magnets placed outside the dynamic flux circuit and producing a field of about 90 kA $m^{-1}$ bias field. A 10 mm-thick coil permits using it against high loads. Due to the magnets and the coil, the diameter, excluding the masses, is about 70 mm. The third actuator, MAS, is biased with cylindrical permanent magnets placed in series between slices of Terfenol-D. The magnet shape have been optimized [16] with FLUX2D [32]. They produce a 90 kA $m^{-1}$ bias field. It also has a 10 mm-thick coil. It is slighty longer than the others, but its diameter is only 50 mm. Some experimental properties of the MB, MAP, MAS drivers are compared in Table 2.

The MAS is an interesting example both from the results and the modelling point of view. It owns the smallest coupling factor. It is due to the series magnets which introduce magnetic reluctances, uncoupled longitudinal compliances and radial stiffnesses [16]. These last mechanical effects cannot be correctly explained by simplified theory (Section 2.2) but they are clearly predicted by ATILA software, as shown in Fig. 5. In spite of these effects, the MAS presents high dynamic strains. The research of the absolute strain limits of linear drivers shows that the highest strains are obtained below resonance. The curve of the absolute maximum strain versus frequency of the unloaded MAS (Fig. 6) has been calculated taking into account both the field limit and the stress limit at each frequency. It defines an optimised law of current which depends on frequency. This new strain curve is above the classical curve of strain at constant current, based on the maximum current acceptable at resonance. It owns a large pass band which might be used in several applications such as active damping, low frequency projectors, etc..

The maximal dissipated energy density is the maximum energy per unit of volume of Terfenol-D which can by dissipated in the load. It is realised in the case of the optimal load. All the experimental values converge to 10–12 kJ $m^{-3}$. This value is between 5 and 10 times higher than that of PZT. It indicates that all these actuators can dissipate 0.4 J providing, for instance at 1 kHz, an output power of 2.5 kW on optimal load.

Linear actuators are studied for building micro-positioners [24,25], fuel injectors [26], fast hydraulic drives [9], high pressure pumps [27], active damping applications [28,29], helicopter blade control [30] etc.. In all of these applications, the expected advantages versus piezoelectric

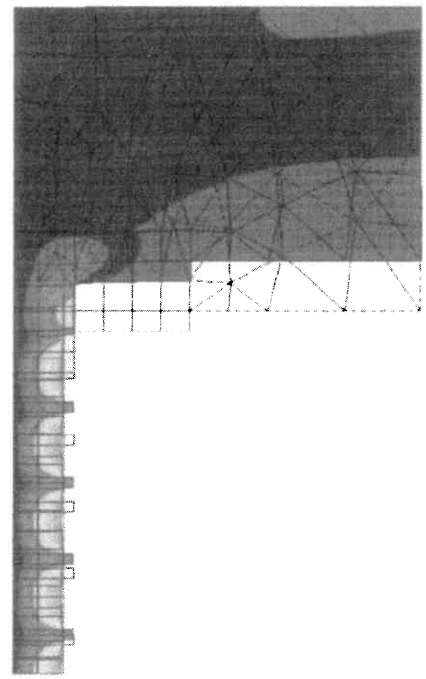

Fig. 5. Deformed shape (continuous lines), structure at rest (dotted lines) and radial displacements (shading) of the MAS, accounting for axial and plane symmetries.

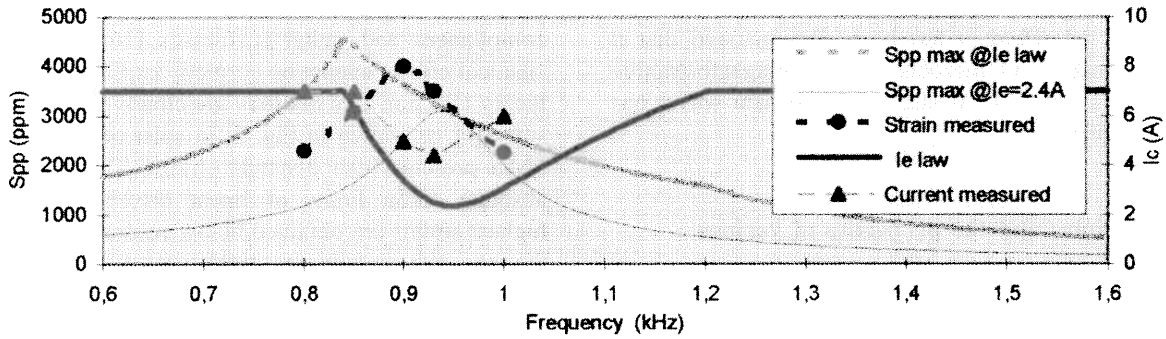


Fig. 6. Calculated curves of MAS: peak-to-peak strain at constant current $I = 2.4$ A, strain with optimised current law, and corresponding current law — measured values of strains of MAS and corresponding currents.

or conventional solutions are the large displacements and large forces associated with low voltages. Their main drawback is the rather high electric power requirement.

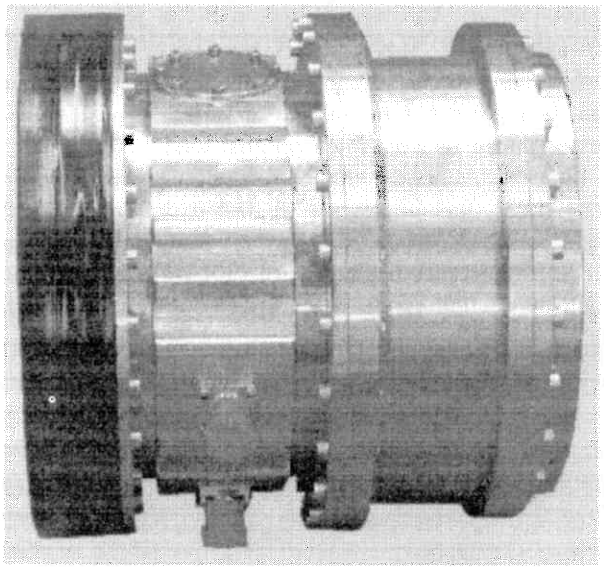

Fig. 7. Sonar transducer tripode.

### 3.2. Transducers

The significance of the giant dynamic strains of Terfenol-D has been grasped rather quickly by transducer designers. Such strain levels, as well as high field limit, high coupling and high compliance, are well suited for high-power transducers both for acoustics (loudspeakers, sonars) [33–35] and for mechanics (welding, sealing, cleaning, machining, cutting, etc.) [5,36]. The Tripode Tonpilz-type sonar transducer [20] (Fig. 7) is a good example for showing the high power capability of Terfenol-D. It is 31 cm long and 30 cm in diameter. It is based on three drivers, each of them including a 100 mm-long, 20 mm in diameter Terfenol-D rod. The maximum theoretical expectation was a headmass displacement of 110 μm, a Terfenol-D strain of 3250 ppm, an output power of 4 kW and a source level of 208.6 dB ref. 1 μPa @ 1 m. Experimentation was performed to achieve about 90% of the theoretical performance. The headmass displacement was measured with an accelerometer giving 98 μm at 1.2 kHz (Fig. 8) corresponding to a 2900 ppm peak-to-peak strain in Terfenol-D. An output power of 3.8 kW and a sound level of 208.1 dB are obtained (Fig. 9). This performance is achieved with an acceptable linearity.

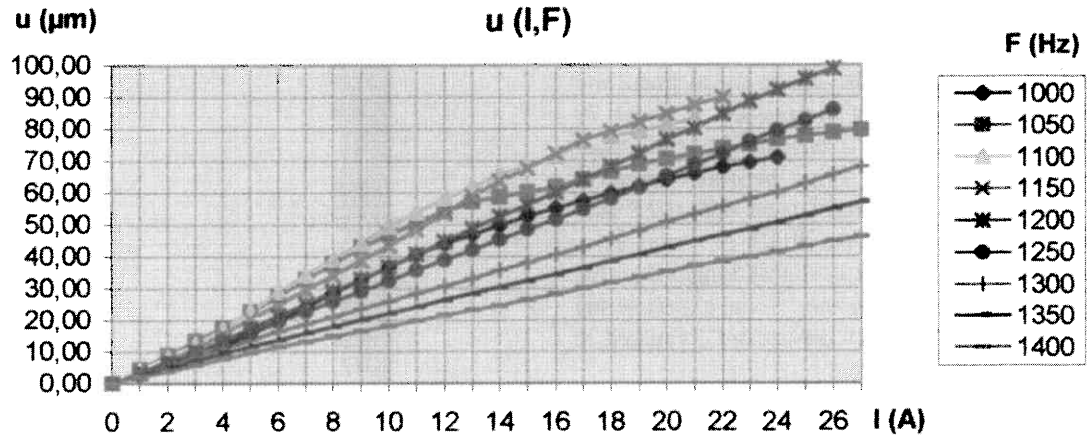


Fig. 8. Displacement of the head mass versus excitation current $I$ at different frequencies.

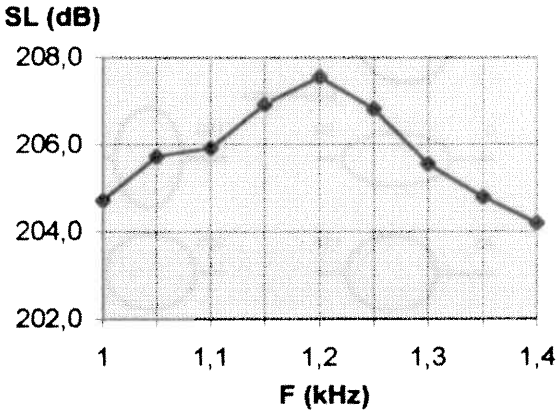


Fig. 9. Tripode measured sound level versus frequency.

High power densities achieved now in Terfenol-D are 10 times higher than those of PZT transducers. These results are interesting knowing that the bias problem is now solved in different ways thanks to specific permanent magnet configurations (Section 3.1) and is being applied [19,37]. Such applications are seen to be promising candidates for development.

### 3.3. Motors

Magnetostrictive linear actuators are able to produce static displacements in the range of 20 to 200 μm. These displacements being larger than mechanical tolerances, they render possible the successful building of inchworm motors [39,38] offering high forces/torques and good resolution, at low speed. These properties are very difficult to obtain with conventional electro-magnetic motors. They need a gear box to obtain high torques which introduce angular play. The efficiency and the wear are their weaknesses and limit the number of applications.

J.M. Vranish [39] has constructed a rotating stepping motor with the highest torque (12.2 Nm) ever reported among all the piezoactive motors. Its holding torque is also very high. Its speed limit (0.5 rpm) is small. Its angular resolution is better than 800 μrad. As is typical with inchworms, its output power is low (<1 W) compared to the electric power required (600 W).

L. Kiesewetter has built an inchworm motor [38] commercialised by Dynamotive in the paper industry. It uses both longitudinal and radial strains in a moving part of a Terfenol-D rod (Fig. 10). Modelling this type of motor [21] provides understanding (Fig. 11). According to Dynamotive, typical results for a motor based on a 120 mm-long 10 mm diameter rod are a maximum speed of 20 mm $s^{-1}$, a maximum force of 1000 N and a resolution of 2 μm.

Friction motors offer a new field of applications for magnetostriction. These motors use the vibrations of a stator to transmit a motion to a rotor or a driven member.

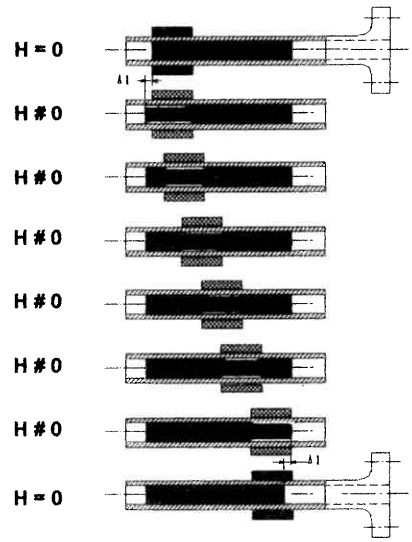


Fig. 10. Kiesewetter motor principle.

Such motors based on piezoelectric ceramics already exist on a large commercial scale. They offer large dynamic and holding torques along with low speeds and good efficiencies due to resonance.

Following a principle used in piezoelectric ultrasonic friction motors [40], T. Akuta [41] has built the first magnetostrictive friction motor. This stator is made of pairs of orthogonal actuators excited with sinusoidal 90° phase shift currents, which produce an elliptical vibration. Modelling of such magnetostrictive stators [22] has shown that in quasi-static operation, a good elliptical motion is produced. It has also been shown that there are many coupled modes, but none of them provides a satisfying elliptical motion. Therefore, unlike piezoelectric motors, this motor cannot operate at resonance. As a consequence and in relation with previous analysis of power (Fig. 4), the efficiency is compulsory weak. Its other characteristics are a speed of 40° $s^{-1}$ and a torque of 1.8 N m [42]. In fact, it is difficult to convert existing piezo-motors to magnetostrictive versions. New designs have to be found.

A first magnetostrictive motor using the mechanical resonance of two vibration modes has been built and tested

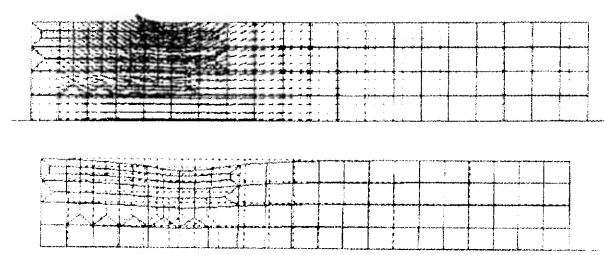

Fig. 11. ATILA computation of $H$-field and strain in the rod of the Kiesewetter motor at one step.

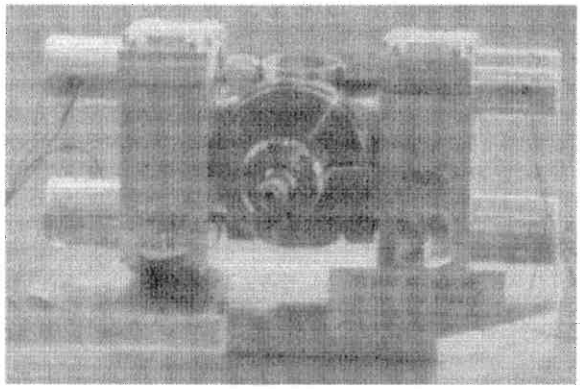

Fig. 12. Multi-mode magnetostrictive FLEX-M1 motor.

by Cedrat Recherche [43] (Fig. 12). Its stator modules are made of a ring and two Terfenol-D linear actuators. The translation mode of the stator produces a vibration which is tangential to the contact zone (Fig. 13(a)). The flexure mode produces a vibration which is normal to the contact zone (Fig. 13(b)). These modes are coupled using a 90° phase shift, in order to produce elliptical vibrations (Fig. 14) which are used to transmit a motion to two rotors by friction. A low rotating speed of $100\,^{\circ}\,s^{-1}$ and a torque of 2.1 N m are achieved (Fig. 15). The goal was to show that Terfenol-D can be used for making high torque motors and that resonance can be beneficial for that purpose and for improving efficiency.

The same principle can be applied to build various kinds of motors according to the number of modules and design choices: linear or rotating, stepping or ultrasonic, etc.. It has been used recently to build an interesting ultrasonic piezomotor [44].

### 3.4. Micro-motors and actuators

T. Fukuda [45] has opened the field of miniature magnetostrictive actuators and motors taking advantage of wireless magnetic excitation. He has experimented with two small self-moving linear motors (some $cm^3$) based on a conversion mode principle.

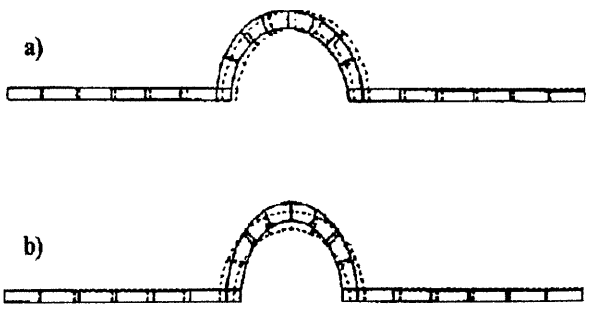


Fig. 13. Vibration modes of a stator module, computed with ATILA: (a) translation mode, (b) flexure mode.

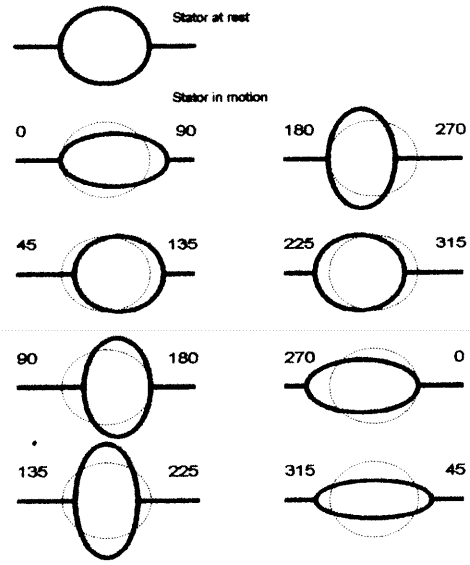


Fig. 14. Principle of FLEX-M1 stator. Stator at rest and in motion versus the actuators phases.

The torsion based, drift free microactuator [46] invented by CNRS, Grenoble, is basically a unimorph structure composed of one magnetostrictive film deposited on a passive substrate. The new feature is a square shape maintained by hinges at three corners (Fig. 16). The useful displacement due to magnetostriction is obtained at the forth free corner, without thermal displacement. The different deformed shapes are due to the anisotropy of magnetostrictive strains and the isotropy of thermal strains. Modelling with ATILA (Figs. 17 and 18) has permitted the design of appropriate micro hinges and the prediction of both shapes. Prototypes have been realised by micro machining a silicon substrate and by depositing a magnetostrictive film by sputtering. Measurements using laser interferometer confirmed the modelling expectations.

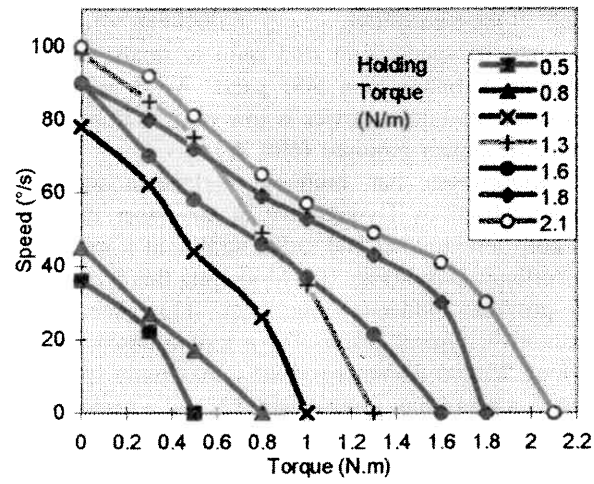


Fig. 15. Measured torque-speed characteristics of FLEX-M1 motor with different holding torques.

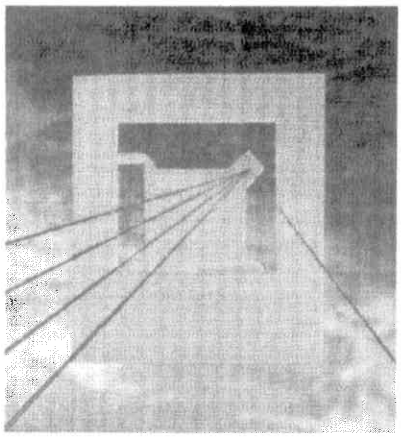

Fig. 16. Magnetostrictive micro-actuator.

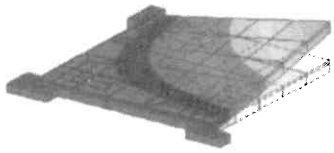

Fig. 17. Magnetostrictive deformation.

Fig. 18. Thermal deformation.

Micromotors currently in study at Cedrat (Figs. 19 and 20) may be classified in the category of the mode conversion ultrasonic motors (MCUM) according to the Japanese classifications of piezomotors, although they are generally not ultrasonic. The motor is a self moving plate including magnetostrictive film. It is submitted to a dynamic field produced by an external coil which may be placed at some cm from the motor. At resonance, this field

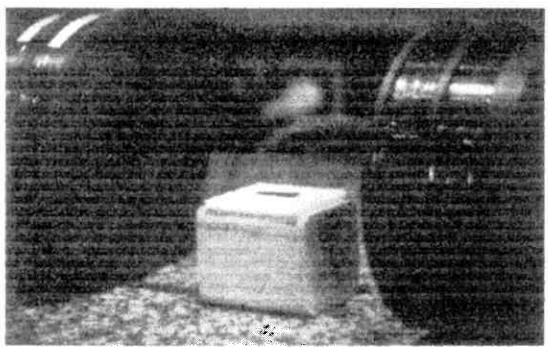

Fig. 19. Wireless linear micro motor.

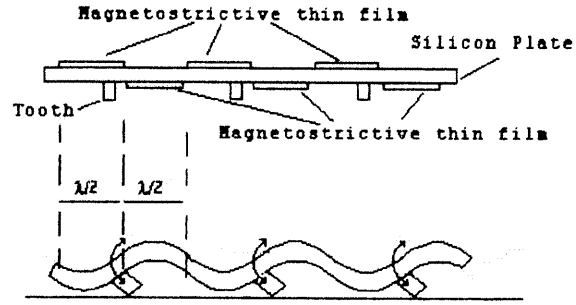


Fig. 20. Principle of the wireless linear micro motor.

excites a flexure mode producing vibrations in the plate, which induces, by friction, a motion at some mm $s^{-1}$.

These examples demonstrate special advantages of magnetostriction, especially the fact that the moving parts are wireless. The disadvantage is the coil which is difficult to make small because of the field requirements. These considerations are driving the development of films with magnetostriction at low field. Note that, as these devices are very small, the price of the material is not a problem. So, such actuators could find large scale applications, for instance in optics, in medicine or in the automobile industry.

## 4. Conclusion

Different methods for designing magnetostrictive devices have been presented. Among these, the 3D finite element model ATILA software appears very general and has been successfully validated several times. Available on PC, it is now ready to be used by engineers. It will permit to improve the design of these devices and will help their development.

Various applications of magnetostriction, especially Terfenol-D, have been studied. Prototypes shows that they provide interesting features. In the case of needs of high output power and due to the giant dynamic strain capability (up to 3500 ppm), magnetostrictive prototypes outperform piezoelectric transducers. Other applications like actuators and motors may also be developed in a larger scale if their cost is reduced. Microsystems may find applications when wireless operation is desired, for instance for reliability.

## Acknowledgments

The authors would like to thank D. Boucher (DCN) and A. Colin, (DRET) for the financial support of Cedrat works on acoustic applications, C. Sol (French ministry of research) for support on electric engineering applications, the European Commission for the financial support on

microsystem applications (BRE2-0536 MAGNIFIT), the partners of MAGNIFIT, especially Laboratory Louis Néel CNRS Grenoble, Kassel universitäte and Forschungszentrum Karlsruhe, for their efforts in producing microsystems and R. Bossut (ISEN) with the team of ISEN acoustic laboratory for their continuous efforts in developing ATILA.

## References

[1] R.M. Bozorth, Ferromagnetism, 2nd ed., Van Nostrand, NY, 1951, 980 pp.
[2] E. De Lacheisserie, Magnetostriction: Theory and Applications, CRC Press, USA, 1993, 410 pp.
[3] A.E. Clark, Magnetostrictive Rare Earth–Fe2 Compounds, Ferromagnetic Materials, E.P. Wohlfarth, US, Tome 1, 1980, pp. 531–588.
[4] J.D. Verhoeven, The effect of composition and magnetic heat treatment on the magnetostriction of TbDyFe twinned single crystals, J. Appl. Phys. 66(2) (1989) 772–779.
[5] L. Sandlung, Magnetostrictive powder composite with high frequency performance, Proc. Third Int. Workshop on Power Transducers for Sonics and Ultrasonics, Springer, FL, 6–8 May, 1992, pp. 113–120.
[6] E. Quandt, Magnetostrictive thin film actuators, Proc. Actuator 94, Axon, Bremen (G), pp. 229–232.
[7] F. Claeyssen, Giant dynamic magnetostrain in rare earth–iron magnetostrictive materials, IEEE Trans. MAG.27, No. 6, Nov. 1991, pp. 5343–5345.
[8] M.B. Moffett, Characterization of Terfenol-D for magnetostrictive transducers, JASA 89(3) (1991) 1448–1455.
[9] L. Kvarnsjö, On characterisation, modelling and application of highly magnetostrictive materials, Doct. Thesis TRITA-EEA-9301, ISSN 1100-1593, 1993, 173 pp.
[10] C. Body, Non-linear finite element modelling of magneto-mechanical phenomenon in giant magnetostrictive thin films, Proc. CEFC, 1996.
[11] G. Engdhal, Loss simulations in magnetostriction actuators, J. Appl. Phys. 79(8) (1996) 00.
[12] ATILA — A 3D CAD software for piezoelectric and magnetostrictive structures, ISEN, Lille (F), Distr. CEDRAT, Meylan (F) and MAGSOFT, Troy NY (US).
[13] J.C. Debus, Finite element modeling of PMN electrostrictive materials, Proc. Int. Conf. on Intelligent Materials, ICIM96-ECSSM96, SPIE vol. 2779, Lyon (F), 1996, pp. 913–916.
[14] F. Claeyssen, Design and building of low-frequency sonar transducers based on rare earth iron magnetostrictive alloys, Doct. Thesis, Defence Research Inform. Cent., HSMO, MoD, London, also Conception et réalisation de transducteurs sonar basse fréquence à base d'alliages magnétostrictifs Terres Rares-Fer, Thèse INSA Lyon, 1989, 414 pp.
[15] F. Claeyssen, Modeling and characterization of the magnetostrictive coupling, Proc. 2nd Int. Workshop on Power Transducers for Sonics and Ultrasonics, Springer, 1990, pp. 132–151.
[16] F. Claeyssen, Giant magnetostrictive alloys actuators, in: L. Lanotte (Ed.), Proc. Magnetoelastic Effects and Applications Conf., Elsevier, Holland, 1993, pp. 153–159, or Journal of Applied Electromagnetics in Materials 5 (1994) 67–73.
[17] P. Bouchilloux, Dynamic shear characterization in a magnetostrictive rare earth–iron alloy, M.R.S. Symp. Proc. 360 (1994) 265–272.
[18] R. Bossut, Finite element modeling of magnetostrictive transducers using ATILA, Proc. ATILA Conf. Joint with 2nd Int. Workshop on Power Transducers for Sonics and Ultrasonics, B.F. Hamonic, Isen, Lille (F), 1990, pp. 19–26.
[19] F. Claeyssen, Progress in magnetostrictive sonar transducers, Proc. UDT93, Reed Exhib., UK, 1993, pp. 246–250.
[20] R. Le Letty, Combined finite element — normal mode expansion methods for ultrasonic motor modeling, IEEE Ultrasonic Symp. Proc, 1994, p. 531–534.
[21] F. Claeyssen, Analysis of magnetostrictive Inchworm motors using f.e.m., In: L. Lanotte, Proc. Magnetoelastic Effects and Applic. Conf., Elsevier, Holland, 1993, pp. 161–167.
[22] F. Claeyssen, State of the art in the field of magnetostrictive actuators, Proc. Actuator 94 conf., Axon, Bremen (G), 1994, pp. 203–209.
[23] Etrema, Terfenol-D Magnetostrictive Actuators Information, Etrema Products, USA, 1993, p. 6.
[24] H. Eda, Ultra precise machine tool with GMA, Ann. of the CIRP 41(1) (1992) 421–424.
[25] W. Wang, A high precision micropositioner based on magnetostriction principle, Rev. Sci. Inst. 63(1) (1992) 249–254.
[26] T. Cedell, New magnetostrictive alloy for rapid conversion of electric energy to mechanical motion, Proc. Actuators 90, Axon, Bremen (G), 1990, pp. 156–161.
[27] K. Suzuki, Magnetostrictive plunger pump, Int. Symp. on GMA and A, Japan, Poster 5, 1992, 6 pp.
[28] M.W. Hiller, Attenuation and transformation of vibration through active control of magnetostrictive Terfenol, J. Sound Vib. 133(3) (1989) 13.
[29] H. Janocha, Design criteria for the application of solid state actuators, Proc. Actuator 94 Conf., Axon, Bremen (G), 1994, pp. 246–250
[30] V. Giurgiutiu, Solid-state actuation of rotor blade servo-flap for active vibration control, J. Int. Mat. Systems Structures 7 (1996) 192–202.
[31] N. Lhermet, Actuators based on biased magnetostrictive rare earth–iron alloys, Proc. Actuator 92, Axon, Bremen (G), 1992, pp. 133–137.
[32] FLUX2D — A 2D CAD software for electric engineering, LEG, Grenoble (F), Distr. CEDRAT, Meylan (F) and MAGSOFT, Troy NY (US).
[33] F. Claeyssen, Design of Lanthanide magnetostrictive sonar projectors, Proc. UDT91, Microwave Exh. and Pub. Ltd, April 1991, pp. 1059–1065.
[34] M.B. Moffett, Comparison of Terfenol-D and PZT4 power limitations, J. Acoust. Soc. Am. 90(2), Letters to editor, August 1991, p. 1184–1185.
[35] D.F. Jones, Recent transduction developments in Canada and US, Sonar Transducers'95 Conf., Proc. Inst. of Acoustics, Univ. of Bath, UK, Vol. 17, Pt. 3, 1995, pp 100–106.
[36] R.J. Wise, Ultrasonic welding of plastics by a Terfenol driven magnetostrictive transducer, Proc of 3rd Conf. on Welding and Adhesive Bonding of Plastic, Dusseldorf, Nov. 1992, pp. 10–12.
[37] B. Dubus, Low frequency magnetostrictive projectors for oceanography and sonar, Proc. 3rd Europ. Conf. on Underwater Acoustics, 1996, pp. 1019–1024.
[38] L. Kiesewetter, Terfenol in linear motor, Proc. of Sec. Int. Conf. on GMA, C. Tyren, Amter (Fr), 1988. Ch. 7, p. 15.
[39] J.M. Vranish, Magnetostrictive direct drive rotary motor development, IEEE Trans. MAG.27, No. 6, Nov. 1991, pp. 5355–5357.
[40] K. Mori, European Patent, No. 0155694A2, 1985.
[41] T. Akuta, Rotational-type actuators with Terfenol-D rods, Proc. Actuators 92, Axon, Bremen (G), 1992, pp. 244–248.
[42] T. Akuta, Improved Rotational-type actuators with Terfenol-D rods, Proc. Actuator 94, Axon, Bremen (G), 1994, pp. 272–274.
[43] F. Claeyssen, Design and construction of a new resonant magnetostrictive motor, Proc. Intermag 96 Conf., Seattle, WA, June 1996, IEEE Trans. MAG, Sept. 96, Vol. 32, No. 5, Part 2, pp. 4749–4751 also Proc. Actuators 96, Axon, Bremen (G), 1996, pp. 172–274.

[44] F. Claeyssen, A new multi-mode piezo-electric motor, Proc. Int. Conf. on Intelligent Materials, ICIM96-ECSSM96, SPIE vol. 2779, Lyon (F), 1996, pp. 634–637 also Proc. Actuators 96, Axon, Bremen (G), 1996, pp. 152–155.

[45] T. Fukuda, GMA applications to micromobile robot as microactuator without power supply cables, IEEE Micro-electro-mechanical Systems Proc. 1991, pp. 210–215.

[46] J. Betz, Torsion based, drift-free magnetostrictive microactuator, Proc. Actuators 96, Axon, Bremen (G), 1996, pp. 283–286.